

## Article

# A Model Surface for Calculating the Reflectance of Smooth and Rough Aluminum Layers in the Vacuum Ultraviolet Spectral Range

Olaf Stenzel <sup>1,2</sup>, Steffen Wilbrandt <sup>1,\*</sup>, Jian-Ying He <sup>1,2</sup>, Sven Stempfhuber <sup>1,2</sup>, Sven Schröder <sup>1</sup> and Andreas Tünnermann <sup>1,2</sup>

<sup>1</sup> Department Functional Surfaces and Coatings, Fraunhofer Institute for Applied Optics and Precision Engineering, Albert-Einstein-Straße 7, 07745 Jena, Germany

<sup>2</sup> Institute of Applied Physics, Friedrich-Schiller-University, Max-Wien-Platz 1, 07743 Jena, Germany

\* Correspondence: [steffen.wilbrandt@iof.fraunhofer.de](mailto:steffen.wilbrandt@iof.fraunhofer.de); Tel.: +49-3641-807272

**Abstract:** We present a systematic approach to calculating the reflectance of aluminum thin films. In our approach, the rough aluminum surface is modelled as a square array of submicrometer-sized oblate cylinders. The focus of the study is on the vacuum ultraviolet (VUV) spectral range, with wavelengths ranging from 120 nm to 200 nm. The VUV reflectance of aluminum films is calculated by using the rigorous coupled wave approach in order to take the surface roughness of aluminum into account. The modelled reflectance spectra are compared to experimental data from unprotected and protected aluminum films.

**Keywords:** aluminum; vacuum ultraviolet; reflectance; surface roughness; absorption; protected mirror; magnesium fluoride



**Citation:** Stenzel, O.; Wilbrandt, S.; He, J.-Y.; Stempfhuber, S.; Schröder, S.; Tünnermann, A. A Model Surface for Calculating the Reflectance of Smooth and Rough Aluminum Layers in the Vacuum Ultraviolet Spectral Range. *Coatings* **2023**, *13*, 122. <https://doi.org/10.3390/coatings13010122>

Academic Editor: Alexandre Botas

Received: 21 December 2022

Revised: 5 January 2023

Accepted: 6 January 2023

Published: 9 January 2023



**Copyright:** © 2023 by the authors. Licensee MDPI, Basel, Switzerland. This article is an open access article distributed under the terms and conditions of the Creative Commons Attribution (CC BY) license (<https://creativecommons.org/licenses/by/4.0/>).

## 1. Introduction

### 1.1. Motivation and Basic Idea of the Study

Aluminum is perhaps the most important metal for use in reflectors for vacuum ultraviolet (VUV) electromagnetic radiation [1]. Numerous studies pursue the optimization of the reflection of aluminum-based mirror coatings, particularly in the wavelength range of approximately 100–200 nm (see for example [2–9]). While unprotected aluminum surfaces suffer considerable absorption losses as the result of the formation of a thin native aluminum oxide overlayer, suitably protected surfaces reach VUV reflectance values in the range between 80% and 90%. Basically, fluorides such as magnesium fluoride [9–12], aluminum fluoride [5,13–15], or lithium fluoride [2,9,12,16,17] have proven useful in protecting aluminum surfaces from oxidation, thereby preventing absorption losses in the oxide overlayer. Limitations in the achievable reflectance may arise from roughness-induced loss mechanisms, which generally include both absorption and scattering contributions. Minimizing the roughness of the mirror coatings therefore appears as a further optimization path for high-performance aluminum-based VUV reflectors. Degradation effects caused by contaminations [18] may also increase the light scattering and chemical reactions with ambient [19–22]. However, degradation effects are not in the scope of this publication, although can have a serious impact to the performance of systems in this spectral range as well [23].

The introduction of Cu substrate [24] or a Ti or Cu seed layer to the aluminum and the resulting effects on the surface quality were shown in [8,25]. It could be demonstrated that the use of the seed layers had an impact on both lateral and vertical characteristic geometrical parameters of the surface profile. Correspondingly, changes in the VUV reflectance of unprotected aluminum surfaces have been observed, while an increase in surface roughness resulted in the typical decrease in reflectance. However, accompanying

simulations in terms of the vector scattering theory have shown that scatter losses must be smaller than 2.5%, and therefore, a considerable amount of the incident VUV light must have been absorbed.

The purpose of the present study is to perform model calculations of the reflectance of rough aluminum surfaces. We will make use of a strongly idealized model surface (periodic in two-dimensions), and we will use rigorous coupled wave analysis (RCWA) for calculating the reflectance [26]. These model calculations will show that a considerable part of the reflection losses may be caused by the absorption of light at the structured interface between the metal and the adjacent dielectric material.

### 1.2. Previously Published Experimental Data Used in this Study

We focus on the VUV reflectance of two different sets of samples that were prepared in a Bühler Syrus Pro 1110 evaporation chamber equipped with a cryogenic and turbomolecular pump. The system is also equipped with two electron guns and a plasma source. The layer thickness and deposition rate were monitored using a quartz crystal.

As substrates, polished silicon (100) wafers with a size of 25 mm × 25 mm and a root mean square (RMS) surface roughness equal to 0.14 nm were used.

The samples from the first set (further unprotected samples) represent a layer system consisting of a seed and an aluminum layer on top. The seed layer materials used were copper and titanium, so there are three different types of samples with one sample type being prepared without seeding as a reference.

For sample preparation, the chamber is heated to a temperature of 80 °C and kept constant during the entire deposition run. After reaching the deposition temperature, there is a waiting period of 300 s. The substrates were cleaned in the chamber by plasma etching for 300 s and a BIAS voltage of 125 V. At a starting pressure  $< 8 \times 10^{-5}$  Pa, the 3 nm-thick seed layer was applied to the substrate: titanium at a rate of 0.02 nm/s and copper at a rate of 0.2 nm/s. Subsequently, a 75 nm aluminum layer was deposited on the seeded substrates with a rate up to 20–25 nm/s. After coating, the aluminum surface was treated with an oxygen plasma for 180 s and 15 sccm oxygen flux to ensure standardized starting conditions of oxidation [8].

The second set of samples (further protected samples) were prepared similar to the first set of samples, but instead of the oxygen plasma treatment at the end, a 5 nm MgF<sub>2</sub> layer was deposited right after the aluminum deposition was finished. This prevents the oxidation of the aluminum surface while the chamber is heated up to a temperature of 225 °C, which is then also kept constant for the last deposition. After reaching the target temperature, a final MgF<sub>2</sub> layer of 22.5 nm thickness was added to the layer system. This deposition routine is described in more detail in [27,28]. Two different types of samples were prepared with this deposition routine, one with a titanium seed layer and one without any seeding acting as a reference.

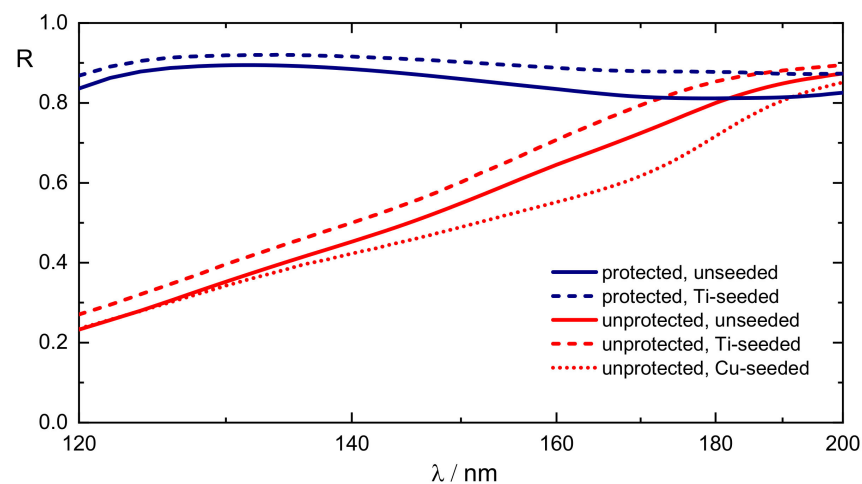
As a basis for realistic modelling, knowledge on a minimum of characteristic geometrical parameters of the aluminum layers is absolutely necessary. If the mentioned two-dimensional RCWA approach requires knowledge of at least one lateral and one vertical parameter characterizing the assumed periodic surface profile, we make use of the otherwise published data (compare [8,29]) on the rms surface roughness as a parameter characterizing the vertical extension of the surface profile, and the average grain sizes as a lateral geometrical parameter. These data are summarized in Table 1.

**Table 1.** Parameters characterizing the surface profile of the mirror coatings.

| Seed Layer | Overlayer  | Average Lateral Aluminum Grain Size/nm | Rms Surface Roughness/nm | $\langle R \rangle_\nu$ |
|------------|--|--|--------------------------|-------------------------|
| none       | Native alumina<br>Protective MgF <sub>2</sub><br>coating | 112                                    | 1.43                     | 0.56                    |
|            |  |  | 1.43                     | 0.85                    |
| Ti         | Native alumina<br>Protective MgF <sub>2</sub><br>coating | 128                                    | 0.38                     | 0.60                    |
|            |  |  | 1.16                     | 0.90                    |
| Cu         | Native alumina   | 56                                     | 1.99                     | 0.51                    |

Note that the rms roughness values reported here are in the range between approximately 0.5 nm and 2.0 nm and thus consistent with data published elsewhere [7].

The Physikalisch Technische Bundesanstalt (PTB), Berlin, carried out reflectivity measurements in the UV-range from 120–220 nm. The measurements were performed at a synchrotron (BESSY) using a VUV reflectometer (PTB, Berlin, Germany). The corresponding measured VUV reflection spectra are shown in Figure 1.

**Figure 1.** Measured VUV normal incidence reflection spectra of the samples specified in Table 1.

As it is obvious from the reflection spectra that magnesium fluoride-protected mirrors (navy lines) have a much larger reflectance than unprotected oxidized surfaces (red lines), although the rms roughnesses are not so different (Table 1). We conclude from here that dominating loss contributions arise from the presence of the native alumina overlayer, while roughness-induced losses provide additional corrections to the total losses. As a trend, larger surface roughness rms values result in a further reduction of the reflectance.

For quantitative ranking, from the reflection spectra, we calculated the average VUV reflectance  $\langle R \rangle_\nu$  according to the recipe:

$$\langle R \rangle_\nu = \frac{\int_{\nu_{min}}^{\nu_{max}} R(\nu) d\nu}{\nu_{max} - \nu_{min}} \quad (1)$$

where  $\nu$  is the wavenumber:

$$\nu = \frac{1}{\lambda} \quad (2)$$

$\lambda$  being the wavelength of the incident light in vacuum. The thus-calculated average reflectances are given in the last column of Table 1 and will later be directly compared to the simulated data. Note the reciprocal abscissa scaling in Figure 1. Due to that abscissa scaling, the presented reflection spectra directly reproduce the spectral shape of  $R(\nu)$ . They differ in shape from corresponding spectra that would be visualized in a linear wavelength scale.

## 2. Idea of Modelling Approach

### 2.1. General

The general idea is to calculate the reflectance of a periodically structured aluminum surface with different types of overlayer. The aluminum film is assumed to be thick enough for preventing any light transmission. The action of possibly different seed layers is only taken into account by differences in the geometrical parameters of the surface structure according to Table 1. Once the transmission is assumed to be zero, in our calculations a simplified energy balance is relevant according to:

$$1 = R + L = R + S + A \quad (3)$$

Here,  $R$  is the reflectance and  $L$  the optical loss. The latter is generally composed from absorption ( $A$ ) and scatter ( $S$ ) contributions. Once we deal with an ideally periodic model surface, the discrete propagating back-diffracted light modes have to be associated with the scatter loss.

Then, in order to have accordance between measured and calculated spectra, we performed simulations for three selected lateral periods  $\Lambda$  of the assumed periodic model structure (compare Table 1):

- $\Lambda = 56$  nm: associated with Cu seeded aluminum films
- $\Lambda = 112$  nm: associated with unseeded aluminum films
- $\Lambda = 128$  nm: associated with Ti seeded aluminum films

In order to visualize the effect of surface roughness for each of these types of layers, reflection spectra have been calculated assuming an rms roughness equal to zero (smooth reference), 0.5 nm; 1.0 nm; 1.5 nm; and 2.0 nm.

Spectra have been calculated at normal light incidence in a spectral range 120–200 nm, assuming vacuum as incident medium. Note that in these conditions, a propagating diffracted light mode can only be observed for the  $\Lambda = 128$  nm structures in the wavelength range 120–128 nm. In all other constellations, any simulated optical loss must be attributed to absorption.

### 2.2. Optical Constants

#### 2.2.1. Aluminum

Due to a lack of VUV spectra of pure (i.e., not oxidized) aluminum films in our lab, we preferred using VUV optical constants of aluminum previously published elsewhere [26,30]. For this study, the optical constants of aluminum as implemented in the UNIGIT database [26] have found application. They are visualized in Figure 2. Here and in the following,  $n$  is the refractive index (i.e., the real part of the complex index of refraction), and  $k$  is the extinction coefficient (i.e., the imaginary part of the complex index of refraction).

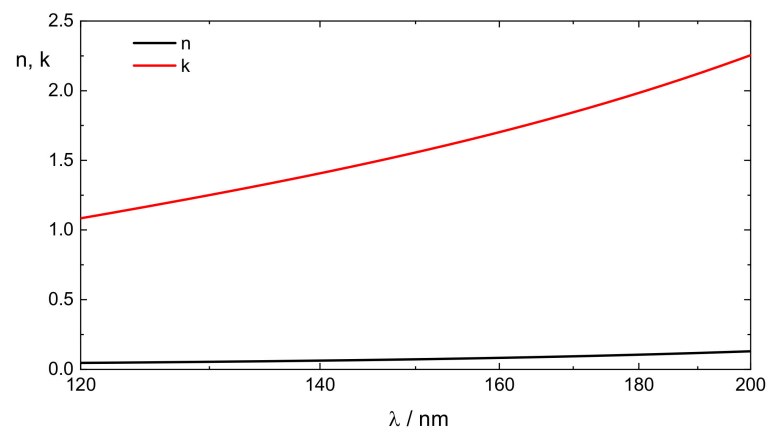


**Figure 2.** VUV optical constants of aluminum.

### 2.2.2. Aluminum Oxide

Once aluminum surfaces exposed to air quickly form an aluminum oxide overlayer, the latter must be taken into account when modelling the VUV reflectance of unprotected aluminum surfaces. This is especially important because of the considerable absorption aluminum oxide shows in the VUV. There are at least two difficulties for realistic modelling:

- The native aluminum oxide films are rather thin, so the determination of their optical constants from VUV reflection spectra of real aluminum surfaces appears unrealistic.
- The exact stoichiometry of the oxide is unclear. This makes it difficult to apply literature data of aluminum oxide to these overlayers. From a previous study [31] we have clear indications that the absorption losses of the native aluminum layer even in the near UV and VIS is considerably larger than would be expected from stoichiometric aluminum oxide. Therefore, in a pragmatic modelling approach, a set of *simulated* optical constants should be applied for modelling the native oxide layer. The challenge is to re-distribute a part of the oscillator strength relevant for stoichiometric alumina VUV absorptions into a broad absorption tail that reaches from the VUV down to the visible spectral region. This will provide the necessary UV absorptions without significantly violating the relevant sum rule [32].

In order to meet this requirement, we decided to make use of Hagemanns [33] published values for stoichiometric aluminum oxide as a starting approximation. These optical constants have then been approximated by a Lorentzian two-oscillator fit in the photon energy range 6–50 eV. The resulting VUV optical constants as used in our study are shown in Figure 3. We obtain model optical constants that somehow smear out the features of Hagemanns original data. In particular, we now observe a broad absorption tail covering a part of the VUV and reaching down to the VIS (red line in Figure 3, note the reciprocal abscissa scaling). As a result, the modelled extinction for wavelength larger than 130 nm is considerably larger than it should be in stoichiometric alumina, which seems to be consistent with the reflectance slope observed in the VUV spectra of unprotected aluminum films. In order to make this difference clear, instead of  $\text{Al}_2\text{O}_3$ , we use the generalized writing  $\text{Al}_x\text{O}_y$ .

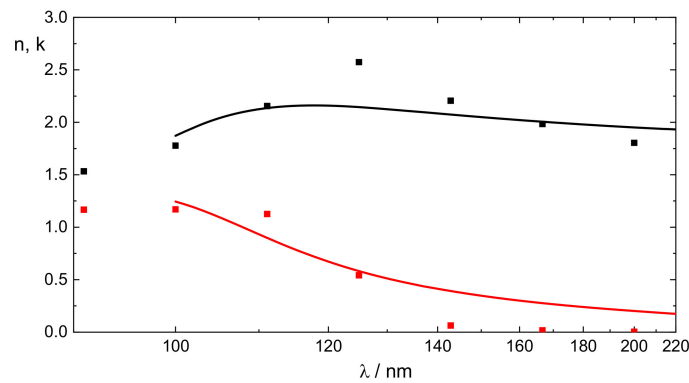


**Figure 3.** Refractive index (black) and extinction coefficient (red) of stoichiometric aluminum oxide (squares) and hypothesis used in our calculations (line).

### 2.2.3. Magnesium Fluoride

The following optical constants from Fraunhofer IOF internal database have been used for the  $MgF_2$  fraction (Figure 4):

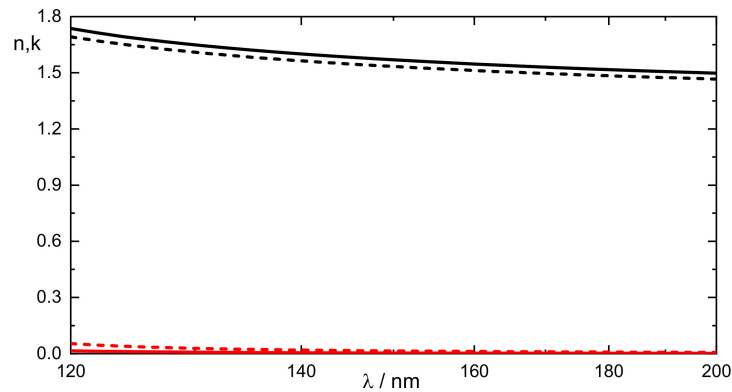


**Figure 4.** VUV Optical constants of  $MgF_2$ ; black: n; red: k; solid lines: deposition at 225 °C, dash: deposition at room temperature.

### 2.3. Surface Profile

#### 2.3.1. RCWA Model

The model surface profile as used in our study is visualized in Figure 5. It consists of regularly arranged aluminum cylinders on an aluminum surface [34]. The diameter of the cylinders is directly related to the lateral period  $\Lambda$ , while the height of the cylinders is additionally related to the rms roughness of the film. The surface element shown in Figure 5 is periodically repeated in both lateral dimensions with the same period  $\Lambda$ . The calculations have been performed using the commercial UNIGIT grating solver software (version 2.02.01). In all calculations, the diameter of the cylinder was set equal to  $0.9 \Lambda$ .

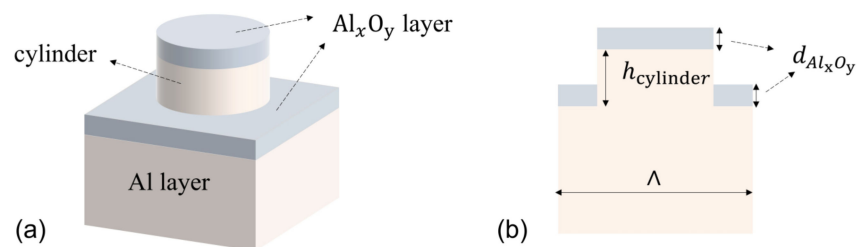


**Figure 5.** (a) Surface element of the native alumina-coated model surface; (b) the same in cross section.

The height  $h$  of all cylinders was identical and chosen such that it results in the respective target rms roughness. From the definition of the rms-roughness  $\sigma$ , the following relation between  $\sigma$  and  $h$  is immediately obtained:

$$h = \frac{\sigma\Lambda^2}{\sqrt{A_{\text{cyl}}(\Lambda^2 - A_{\text{cyl}})}} \quad (4)$$

where  $A_{\text{cyl}}$  is the ground area of the cylinder. For a cylinder diameter of  $0.9\Lambda$ , this results in:

$$h \approx 2.078\sigma \quad (5)$$

Depending on the system to be modeled, the described surface is assumed to be covered by either aluminum oxide or magnesium fluoride. Note that our RCWA software (version 2.02.01) is unable to introduce conformal coating in such a geometry, and therefore, provided that the cylinder height  $d_{\text{cylinder}}$  is larger than the assumed thickness of the aluminum oxide  $d_{\text{Al}_x\text{O}_y}$ , a part of the aluminum surface appears to be in direct contact with vacuum, which is a model artefact that we have to accept. We will return to that point later in the discussion.

### 2.3.2. Relation of Model Systems to Real Systems

Table 2 defines the correspondence between model systems and their real counterparts, if available (crosses):

$$a|_{\text{max}} = \frac{h_{\text{cylinder,max}}}{\Lambda_{\text{min}}} \approx 0.072 \quad (6)$$

and, thus, well below 10%. We conclude from here that we may expect quick convergence of the RCWA calculation procedure. As we have tested in terms of truncation runs, convergence was generally achieved when the RCWA calculation was performed considering a maximum of 8 Rayleigh orders.

**Table 2.** Correspondence between simulated systems and real samples.

| $\Lambda/\text{nm}$ | $h_{\text{cylinder}}/\sigma/$   | Overlayer |       |       |       |       | Attributed System   |
|---------------------|---|-----------|-------|-------|-------|-------|---|
|                     |   | 0         | 1.039 | 2.078 | 3.177 | 4.156 |   |
|                     |   | 0         | 0.5   | 1     | 1.5   | 2     |   |
| 56<br>112<br>128    | None  |           |       |       |       |       | Theoretical reference   |
| 56<br>112<br>128    | 5 nm <sup>(1)</sup><br>MgF <sub>2</sub> +<br>22.5 nm <sup>(2)</sup><br>MgF <sub>2</sub> |           |       | x     |       |       | Cu seeded protected <sup>(3)</sup><br>Unseeded protected<br>Ti seeded protected |
| 56<br>112<br>128    | 2.5 nm Al <sub>x</sub> O <sub>y</sub>   |           |       |       | x     |       | Cu seeded unprotected<br>Unseeded unprotected<br>Ti seeded unprotected          |

<sup>(1)</sup> deposition at room temperature; <sup>(2)</sup> deposition at 225 °C; <sup>(3)</sup> not manufactured. Note that the largest assumed cylinder height is about 4 nm, and the smallest period is 56 nm. The maximum aspect ratio  $a|_{\text{max}}$  is then about:

Let us emphasize in that context that our primary goal is to study the VUV reflectance of a periodic model surface with spatial parameters close to the measured data presented in Table 1. It is a specific feature of our model that the surface profile is defined by regularly

arranged free-standing oblate cylindrical units with a diameter slightly smaller than the assumed period. The reason for this is that, in our model, both the lateral period and cylinder diameter are chosen to be close to the measured lateral aluminum grain sizes reported in Table 1. On the other hand, if the cylinders were to come into direct contact with each other, we would expect extraordinarily large local electric field strengths in the surface structure, which could—as a worst-case scenario—impair the convergence of the RCWA calculations. Therefore, the choice of a cylinder diameter of  $0.9\Lambda$  appears as a reasonable compromise. Nevertheless, that choice is arbitrary, and another chosen relation between the diameter and period while keeping the rms roughness constant would result in other cylinder heights, other aspect ratios, and finally other reflectance spectra.

### 3. Results

#### 3.1. Smooth Layers

In the special case of smooth surfaces, the optical constants given in Figures 2–4 allow for calculating the VUV reflectance in terms of the typical thin film matrix formalism [32]. Figure 6 shows the results for a hypothetical pure aluminum surface (black), an aluminum surface covered by 2.5 nm aluminum oxide (red) with optical constants according to Figure 3, as well as an aluminum surface protected by an  $\text{MgF}_2$  film (green). In fact, the optical constants of magnesium fluoride films depend on the deposition temperature, and therefore, the magnesium fluoride protective coating has been modelled as a two-layer system as described given in Table 2, by using the optical constants shown in Figure 4.

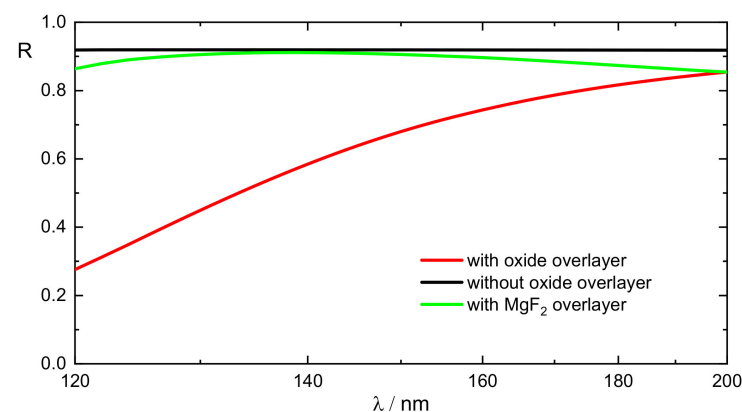


**Figure 6.** Calculated VUV-reflectance of different smooth aluminum surfaces.

Astonishingly, the thus-simulated reflection spectra are already qualitatively similar to their respective measured counterparts from Figure 1. Thus, the  $\text{MgF}_2$ -protected surface has a rather high reflectance that comes close to that of the hypothetical pure aluminum surface. The unprotected but oxidized surface has a considerably smaller reflectance, with a slope close to what has been found in the measurement. This is a further indication that the decreased reflectance of oxidized aluminum surfaces is mainly caused by absorption in the oxide overlayer, and only to a significantly smaller amount by roughness-induced loss mechanisms.

#### 3.2. Rough Layers

##### 3.2.1. Effect of Increasing Period

In order to highlight the impact of different geometrical surface profile parameters, in Figure 7 we present the reflection spectra of three systems that differ only in the lateral period  $\Lambda$ . The picture shows simulated spectra of aluminum surfaces overcoated with 2.5 nm alumina, all having the same rms surface roughness  $\sigma = 2$  nm. As a trend, a larger period results in a slightly increased average reflectance. This agrees with the empirically established general trend, that laterally larger grains in a metal film tend to result in a larger reflectance (compare Reference [35]).

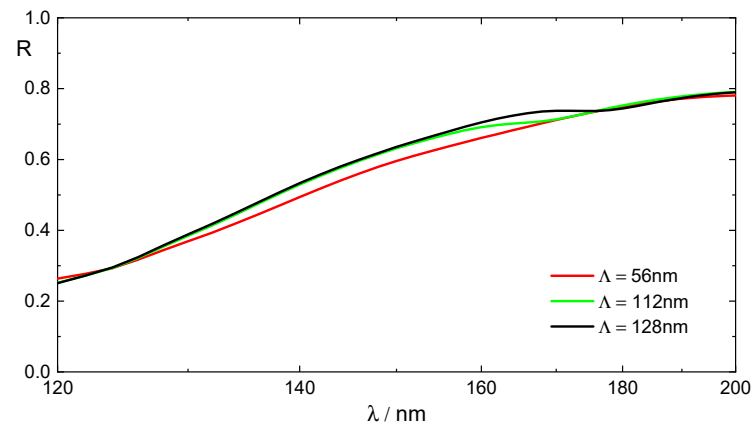


**Figure 7.** Calculated VUV reflectance of unprotected aluminum films with  $\sigma = 2$  nm, and different periods  $\Lambda$ .

### 3.2.2. Effect of Increasing Rms Roughness

In contrast to the previous situation, Figure 8 presents a set of reflection spectra arising from oxidized aluminum surface with the same lateral period  $\Lambda = 56$  nm, but a different rms roughness  $\sigma$ . As a trend, when the lateral period is fixed, an increase in the roughness results in a decreased reflectance, which coincides with the common experience.

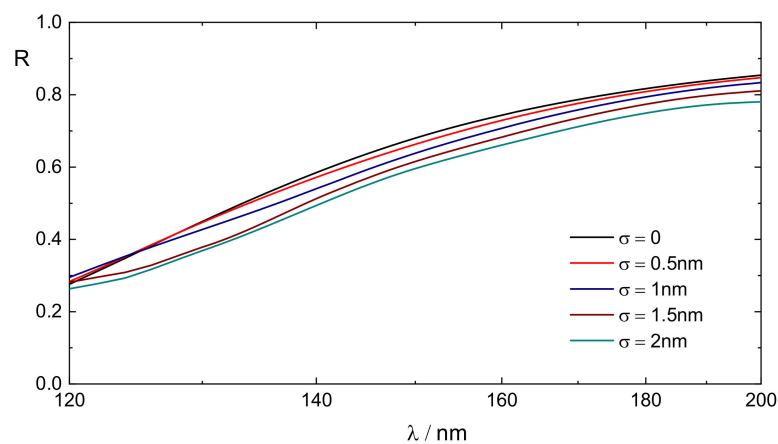


**Figure 8.** Calculated VUV reflectance of unprotected aluminum films with  $\Lambda = 56$  nm and different rms roughnesses  $\sigma$ .

### 3.3. Propagating Diffracted Modes

In the considered spectral range, first order propagating back-diffracted modes are only allowed for the samples with  $\Lambda = 128$  nm. Corresponding diffraction intensities  $R_{diff}$  are presented in Figure 9. In these calculations, the rms surface roughness was set to a hypothetical value of 2 nm. A maximum diffraction efficiency of 4% has been found, however real surface roughnesses as obtained from Ti-seeded samples were in the range of 1 nm or smaller (Table 1). Therefore, the maximum diffraction efficiency should be around 2% for those of our model surfaces which represent counterparts of the real samples.

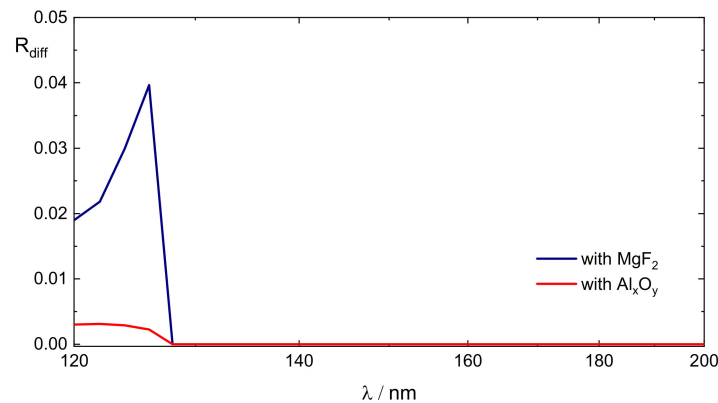


**Figure 9.** Calculated diffraction efficiencies for model surfaces with  $\sigma = 2$  nm and  $\Lambda = 128$  nm.

#### 4. Discussion

##### 4.1. Comparison with Experiment and Limits of the Model

Figure 10 provides a direct comparison between experimental spectra (left) and their calculated counterparts (right), i.e., calculated spectra from surface structures with geometrical parameters that fall closest to those collected in Table 1.

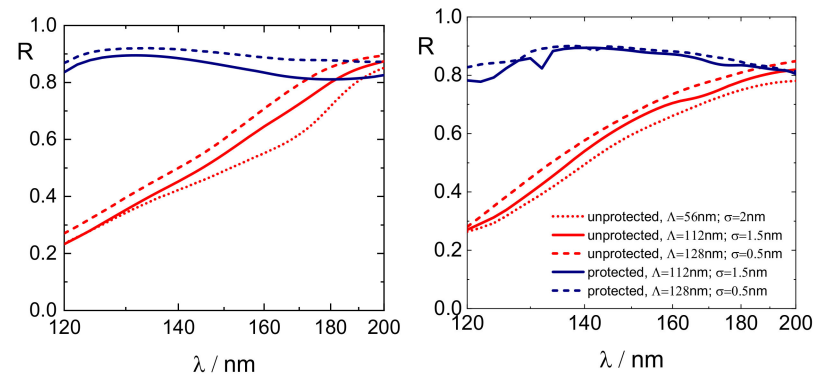


**Figure 10.** Left: measured VUV-spectra; right: selected calculated spectra.

In comparing these two graphs, we would like to emphasize two points:

- There is a good qualitative agreement between the measured spectra and their calculated counterparts. In particular, the calculated reflectance ranking coincides with the measured one.
- There are clear differences when comparing specific spectral features. Thus, in one of the simulated spectra of a protected surface, we see a surface plasmon resonance around a wavelength of 132 nm, which is absent in the experimental spectra. We see a basic reason for this discrepancy in the highly idealized assumed surface structure, in particular the assumed strong periodicity, which results in an identical assumed size of all cylinders. In reality, due to the statistical distribution of the sizes of surface structure elements, such spectral features caused by surface plasmon excitation will smear out.

Once the RCWA is limited in application to periodic structures, in the frames of this study, we cannot eliminate the second point. In order to take advantage of the first point, in the following, the discussion is focused on the comparison of spectrally averaged VUV reflectances. This way we try to keep the information about the ranking of the samples with regard to their reflectance while averaging out those spectral features that are caused by specific geometrical features.

#### 4.2. Spectrally Averaged VUV Reflectances

The Tables 3–5 present average reflectances corresponding to all measured and calculated reflection spectra. In addition to  $\langle R \rangle_\nu$  as calculated according to (1) and (2), the tables also show—for the sake of completeness—reflectances averaged in wavelength scaling. The latter are calculated according to (7):

$$\langle R \rangle_\lambda = \frac{\int_{\lambda_{min}}^{\lambda_{max}} R(\lambda) d\lambda}{\lambda_{max} - \lambda_{min}} \quad (7)$$

**Table 3.** Averaged calculated reflectances for assumed pure aluminum surfaces for simulated lateral periods  $\Lambda$  and roughnesses  $\sigma$ .

| $\sigma/\text{nm}$ | $\Lambda/\text{nm}$         |                         |                             |                         |                             |                         |
|--------------------|-----------------------------|-------------------------|-----------------------------|-------------------------|-----------------------------|-------------------------|
|                    | 56                          |                         | 112                         |                         | 128                         |                         |
|                    | $\langle R \rangle_\lambda$ | $\langle R \rangle_\nu$ | $\langle R \rangle_\lambda$ | $\langle R \rangle_\nu$ | $\langle R \rangle_\lambda$ | $\langle R \rangle_\nu$ |
| 0                  | 0.919                       | 0.924                   | 0.919                       | 0.924                   | 0.919                       | 0.924                   |
| 0.5                | 0.904                       | 0.906                   | 0.909                       | 0.912                   | 0.909                       | 0.912                   |
| 1                  | 0.869                       | 0.871                   | 0.887                       | 0.889                   | 0.890                       | 0.895                   |
| 1.5                | 0.820                       | 0.830                   | 0.857                       | 0.865                   | 0.862                       | 0.871                   |
| 2                  | 0.764                       | 0.784                   | 0.821                       | 0.836                   | 0.829                       | 0.842                   |

**Table 4.** Averaged reflectances for unprotected (i.e., alumina-coated) aluminum surfaces for simulated lateral periods  $\Lambda$  and roughnesses  $\sigma$  and available experimental results.

| $\sigma/\text{nm}$ | $\Lambda/\text{nm}$         |                         |                             |                         |                             |                         |
|--------------------|-----------------------------|-------------------------|-----------------------------|-------------------------|-----------------------------|-------------------------|
|                    | 56                          |                         | 112                         |                         | 128                         |                         |
|                    | $\langle R \rangle_\lambda$ | $\langle R \rangle_\nu$ | $\langle R \rangle_\lambda$ | $\langle R \rangle_\nu$ | $\langle R \rangle_\lambda$ | $\langle R \rangle_\nu$ |
| 0                  | 0.682                       | 0.632                   | 0.682                       | 0.632                   | 0.682                       | 0.632                   |
| 0.5                | 0.673                       | 0.626                   | 0.675                       | 0.626                   | 0.675                       | 0.626                   |
| 1                  | 0.655                       | 0.608                   | 0.662                       | 0.614                   | 0.663                       | 0.614                   |
| 1.5                | 0.628                       | 0.579                   | 0.642                       | 0.591                   | 0.645                       | 0.596                   |
| 2                  | 0.607                       | 0.561                   | 0.623                       | 0.573                   | 0.6275                      | 0.579                   |
|                    | Experiment                  |                         |                             |                         |                             |                         |
| 1.99               | 0.561                       | 0.509                   | -                           | -                       | -                           | -                       |
| 1.43               | -                           | -                       | 0.615                       | 0.56                    | -                           | -                       |
| 0.38               | -                           | -                       | -                           | -                       | 0.664                       | 0.602                   |

**Table 5.** Averaged reflectances for protected (i.e., MgF<sub>2</sub>-coated) aluminum surfaces for simulated lateral periods  $\Lambda$  and roughnesses  $\sigma$  and available experimental results.

| $\sigma/\text{nm}$ | $\Lambda/\text{nm}$         |                         |                             |                         |                             |                         |
|--------------------|-----------------------------|-------------------------|-----------------------------|-------------------------|-----------------------------|-------------------------|
|                    | 56                          |                         | 112                         |                         | 128                         |                         |
|                    | $\langle R \rangle_\lambda$ | $\langle R \rangle_\nu$ | $\langle R \rangle_\lambda$ | $\langle R \rangle_\nu$ | $\langle R \rangle_\lambda$ | $\langle R \rangle_\nu$ |
| 0                  | 0.888                       | 0.895                   | 0.888                       | 0.895                   | 0.888                       | 0.895                   |
| 0.5                | 0.871                       | 0.877                   | 0.877                       | 0.883                   | 0.877                       | 0.883                   |
| 1                  | 0.851                       | 0.86                    | 0.863                       | 0.871                   | 0.863                       | 0.865                   |
| 1.5                | 0.832                       | 0.836                   | 0.848                       | 0.854                   | 0.846                       | 0.848                   |
| 2                  | 0.812                       | 0.813                   | 0.8305                      | 0.83                    | 0.828                       | 0.83                    |
|                    | Experiment                  |                         |                             |                         |                             |                         |
| 1.16               | -                           | -                       | -                           | -                       | 0.892                       | 0.895                   |
| 1.43               | -                           | -                       | 0.844                       | 0.854                   | -                           | -                       |

In practice the data  $\langle R \rangle_\lambda$  according to (7) have been calculated by straightforward numerical integration of the measured VUV spectra  $R(\lambda)$ . Therefore, according to (2), we have:

$$dv = -\frac{1}{\lambda^2}d\lambda; \lambda_{min} = \frac{1}{\nu_{max}}; \lambda_{max} = \frac{1}{\nu_{min}} \tag{8}$$

The calculation of  $\langle R \rangle_\nu$  according to (1) has been accomplished by numerical integration of the same VUV-spectra using the recipe:

$$\langle R \rangle_\nu = \frac{\int_{\nu_{min}}^{\nu_{max}} R(\nu)d\nu}{\nu_{max} - \nu_{min}} = -\frac{\int_{\lambda_{max}}^{\lambda_{min}} \frac{R(\lambda)}{\lambda^2}d\lambda}{\frac{1}{\lambda_{min}} - \frac{1}{\lambda_{max}}} = \lambda_{max}\lambda_{min} \frac{\int_{\lambda_{min}}^{\lambda_{max}} \frac{R(\lambda)}{\lambda^2}d\lambda}{\lambda_{max} - \lambda_{min}} \tag{9}$$

The practical sense of distinguishing between the average reflectances calculated according to (7) and (9) is as follows. Assume first that the reflectance  $R(\lambda)$  is independent on the wavelength (or wavenumber). In this case, (7) and (9) will naturally provide identical results coinciding with the assumed constant reflectance value. If, however the reflectance tends to decrease with a decreasing wavelength, then, as a result of the additional  $\lambda^{-2}$  term in the integrand,  $\langle R \rangle_\nu$  according to (1) or (9) will be smaller than  $\langle R \rangle_\lambda$  calculated according to (7). This is obviously the case for unprotected samples and is reflected in the data from Table 4. On the contrary, when the reflectance tends to increase with decreasing wavelength, we find that  $\langle R \rangle_\nu > \langle R \rangle_\lambda$ . Distinguishing between the two types of reflectance averages thus provides a quick-and-dirty method for recognizing the basic wavelength trend of the reflectance. This also explains the different relationship between  $\langle R \rangle_\nu$  and  $\langle R \rangle_\lambda$  as obtained for different kinds of samples (Tables 3–5).

A graphical visualization of the data from Tables 3–5 vs.  $\sigma$  is provided in Figure 11. Experimental data for the unprotected and protected aluminum surfaces are indicated by black symbols (triangles: unseeded layer; circle: Ti seed layer; and star: Cu seed layer). Different lateral periods  $\Lambda$  in the simulation data are indicated by the dashed lines, where “red” corresponds to  $\Lambda = 56$  nm; “green” to  $\Lambda = 112$  nm; and “blue” to  $\Lambda = 128$  nm. We recognize a general trend towards smaller reflectances (i.e., higher losses) when the period decreases down to 56 nm. This is contrary to what would be expected for scatter losses.

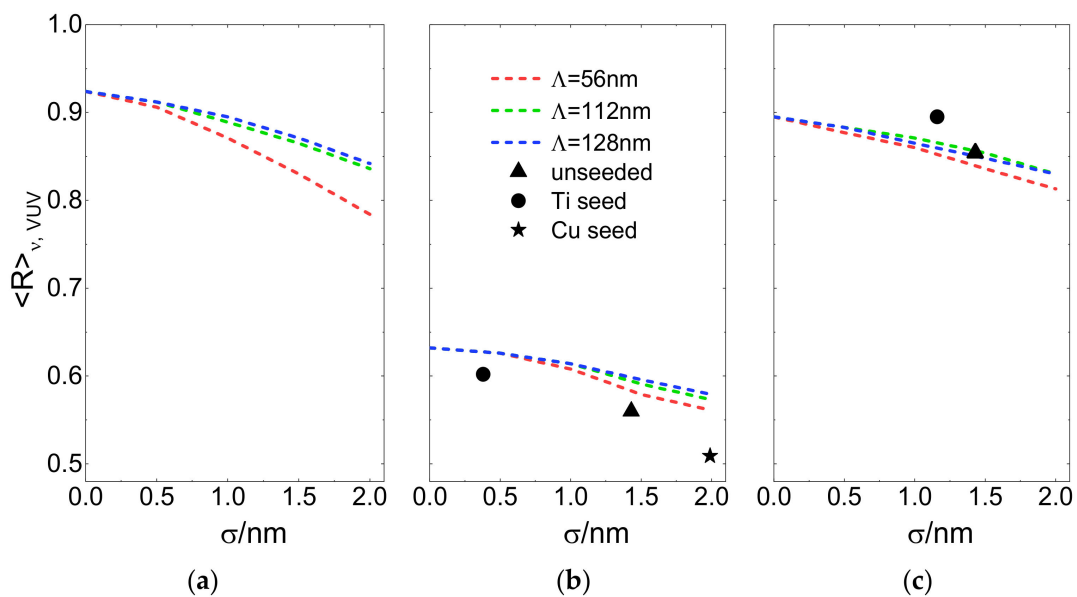


**Figure 11.** Comparison between average VUV reflectance data. Dashed lines represent calculated dependencies and symbols experimental data. Details see text. (a) pure aluminum, (b) unprotected aluminum, and (c) protected aluminum.

We also recognize a general decrease in reflectance when  $\sigma$  is increased, a rather expected behavior for a roughness-induced optical loss mechanism. All in all, an increase of  $\sigma$  from 0 to 2 nm leads to reflection losses of approximately 10% in all groups of samples. Once the largest assumed lateral period in our model surfaces was 128 nm; this calculated additional loss is again mainly caused by absorptions in the corrugated aluminum surface. This is in qualitative agreement with estimations of the scatter loss published earlier in [8], where scatter losses considerably smaller than 10% have been calculated.

We mention here that our calculations do not reproduce the high measured reflectance of the Ti-seeded protected sample (circle in Figure 11b). Indeed, its reflectance comes close to that of a pure aluminum surface. A reason could be in a large porosity of the MgF<sub>2</sub> layer, which would result in a decrease of its refractive index.

The remaining discrepancies between calculated and measured reflectance data may be attributed to the strong simplifications accepted when defining the model surface. To our opinion, there are at least two simplifications that lead to an overestimation of the reflectance in our calculations:

- The assumed strong periodicity does not allow for scatter losses when the wavelength is larger than the assumed period. This is in contrast to real stochastic surface profiles, which are expected to show scatter losses and therefore a somewhat smaller specular reflectance.
- The impossibility of modelling conformal coating with native alumina results in an underestimation of the amount of alumina in the detection volume when the cylinder height is larger than the assumed alumina thickness (compare Figure 5). Once the alumina is strongly absorbing in the VUV, this effect results in an additional overestimation of the reflectance in the case of unprotected layers when comparing with measured values. The discrepancy should increase with increasing roughness, which is indeed observed in Figure 11. In the case of our model surface, this effect is not so relevant for the quantitative results, because even in the worst-case scenario of the lowest period  $\Lambda = 56$  nm combined with the largest roughness of  $\sigma = 2$  nm, the amount of pure aluminum surface merely constitutes 6.5% of the full surface. In real stochastic structures, however, the conformal alumina coating of all surface structures may result in a rather significant increase of the alumina amount in the detection volume, which gives a qualitative explanation to the measured larger reflectance losses when the surface roughness of unprotected layers is increased.

## 5. Summary

The main results of the study can be summarized as follows:

1. The VUV normal incidence reflectance of protected and unprotected aluminum mirrors was calculated by the RCWA, assuming a two-dimensional periodic surface profile with regularly arranged cylinders with a height that is related to typical rms surface values of evaporated aluminum layers.
2. MgF<sub>2</sub>-protected aluminum surfaces have an average measured VUV reflectance around 85%–90%, while unprotected films have an average reflectance around 50%–60%. This order of magnitude may be reproduced in the calculations when assuming that the unprotected films are covered by a 2.5 nm-thick native alumina layer. The loss in reflectance is therefore mainly attributed to absorption losses in the alumina overlayer.
3. An increase in the rms surface roughness from 0 to 2 nm leads to an additional decrease in the average reflectance of around 10%. According to our calculations, these 10% are the optimization potential when maximizing the VUV reflectance by improving the surface quality, for example by applying seed layers.

**Author Contributions:** Conceptualization, O.S.; methodology, O.S., S.W., J.-Y.H., S.S. (Sven Stempfhuber) and A.T.; validation, all authors; formal analysis, all authors; investigation, O.S., S.W., J.-Y.H. and S.S. (Sven Stempfhuber); resources, O.S., S.W., J.-Y.H., and S.S. (Sven Stempfhuber); data curation, O.S., S.W., J.-Y.H. and S.S. (Sven Stempfhuber); writing—original draft preparation, O.S.; writing—review and editing, all authors; visualization, O.S., S.W., S.S. (Sven Stempfhuber) and J.-Y.H.; supervision, O.S.; project administration, S.W.; funding acquisition, S.W., O.S., S.S. (Sven Schröder) and A.T. All authors have read and agreed to the published version of the manuscript.

**Funding:** The study was partially funded by Fraunhofer internal project Multi-KID (Grant No. 601001).

**Institutional Review Board Statement:** Not applicable.

**Informed Consent Statement:** Not applicable.

**Data Availability Statement:** Not applicable.

**Conflicts of Interest:** The authors declare no conflict of interest.

## References

1. Hass, G.; Tousey, R. Reflecting Coatings for the Extreme Ultraviolet. *J. Opt. Soc. Am.* **1959**, *49*, 593. [[CrossRef](#)]
2. Hunter, W.R.; Osantowski, J.F.; Hass, G. Reflectance of Aluminum Overcoated with MgF(2) and LiF in the Wavelength Region from 1600 Å to 300 Å at Various Angles of Incidence. *Appl. Opt.* **1971**, *10*, 540–544. [[CrossRef](#)] [[PubMed](#)]
3. Hass, G. Filmed Surfaces for Reflecting Optics. *J. Opt. Soc. Am.* **1955**, *45*, 945. [[CrossRef](#)]
4. Canfield, L.R.; Hass, G.; Waylonis, J.E. Further studies on MgF(2)-overcoated aluminum mirrors with highest reflectance in the vacuum ultraviolet. *Appl. Opt.* **1966**, *5*, 45–49. [[CrossRef](#)]
5. Gutiérrez-Luna, N.; Perea-Abarca, B.; Espinosa-Yáñez, L.; Honrado-Benítez, C.; de Lis, T.; Rodríguez-de Marcos, L.V.; Aznárez, J.A.; Larruquert, J.I. Temperature Dependence of AlF<sub>3</sub> Protection on Far-UV Al Mirrors. *Coatings* **2019**, *9*, 428. [[CrossRef](#)]
6. Quijada, M.A.; Del Hoyo, J.; Gray, E.; Richardson, J.G.; Howe, A.; Rodríguez de Marcos, L.; Sheikh, D. Influence of evaporation rate and chamber pressure on the FUV reflectance and physical characteristics of aluminum films. In Proceedings of the UV/Optical/IR Space Telescopes and Instruments: Innovative Technologies and Concepts X, San Diego, CA, USA, 1–5 August 2021; Breckinridge, J.B., Stahl, H.P., Barto, A.A., Eds.; SPIE: Bellingham, WA, USA, 2021; p. 18, ISBN 9781510644762.
7. Wilbrandt, S.; Stenzel, O.; Nakamura, H.; Wulff-Molder, D.; Duparré, A.; Kaiser, N. Protected and enhanced aluminum mirrors for the VUV. *Appl. Opt.* **2014**, *53*, A125–A130. [[CrossRef](#)] [[PubMed](#)]
8. Stempfhuber, S.; Felde, N.; Schwinde, S.; Trost, M.; Schenk, P.; Schröder, S.; Tünnermann, A. Influence of seed layers on optical properties of aluminum in the UV range. *Opt. Express* **2020**, *28*, 20324–20333. [[CrossRef](#)] [[PubMed](#)]
9. Hutcheson, E.T.; Hass, G.; Cox, J.T. Effect of Deposition Rate and Substrate Temperature on the Vacuum Ultraviolet Reflectance of MgF(2)- and LiF-Overcoated Aluminum Mirrors. *Appl. Opt.* **1972**, *11*, 2245–2248. [[CrossRef](#)]
10. de Marcos, L.V.R.; Larruquert, J.I.; Méndez, J.A.; Gutiérrez-Luna, N.; Espinosa-Yáñez, L.; Honrado-Benítez, C.; Chavero-Royán, J.; Perea-Abarca, B. Optimization of MgF<sub>2</sub>-deposition temperature for far UV Al mirrors. *Opt. Express* **2018**, *26*, 9363–9372. [[CrossRef](#)]
11. Fernández-Perea, M.; Larruquert, J.I.; Aznárez, J.A.; Pons, A.; Méndez, J.A. Vacuum ultraviolet coatings of Al protected with MgF(2) prepared both by ion-beam sputtering and by evaporation. *Appl. Opt.* **2007**, *46*, 4871–4878. [[CrossRef](#)]
12. Adriaens, M.R.; Feuerbacher, B. Improved LiF and MgF(2) Overcoated Aluminum Mirrors for Vacuum Ultraviolet Astronomy. *Appl. Opt.* **1971**, *10*, 958–959. [[CrossRef](#)] [[PubMed](#)]
13. Rodríguez-de Marcos, L.V.; Boris, D.; Del Hoyo, J.; Wheeler, V.; Woodward, J.; Richardson, G.; Walton, S.; Wollack, E.; Quijada, M. Advanced AlF<sub>3</sub>-passivated Aluminum mirrors for UV astronomy. In Proceedings of the Astronomical Optics: Design, Manufacture, and Test of Space and Ground Systems III, San Diego, CA, USA, 1–5 August 2021; Hallibert, P., Hull, T.B., Kim, D., Keller, F., Eds.; SPIE: Bellingham, WA, USA, 2021; p. 1, ISBN 9781510644786.
14. Boris, D.R.; Rodríguez-de Marcos, L.V.; Del Hoyo, J.G.; Wheeler, V.D.; Walton, S.G.; Wollack, E.J.; Quijada, M.A. Plasma based production of AlF<sub>3</sub>-passivated aluminum mirrors for UVOIR astronomy. In Proceedings of the Space Telescopes and Instrumentation 2022: Ultraviolet to Gamma Ray, Montréal, QC, Canada, 17–23 July 2022; den Herder, J.-W.A., Nakazawa, K., Nikzad, S., Eds.; SPIE: Bellingham, WA, USA, 2022; p. 124, ISBN 9781510653436.
15. Fronk, K.; Allred, D.D. Evidence that evaporated Al/AlF<sub>3</sub> bilayer thin films stored in a 327 K oven for over 2500 h have not degraded. In Proceedings of the Space Telescopes and Instrumentation 2022: Ultraviolet to Gamma Ray, Montréal, QC, Canada, 17–23 July 2022; den Herder, J.-W.A., Nakazawa, K., Nikzad, S., Eds.; SPIE: Bellingham, WA, USA, 2022; p. 122, ISBN 9781510653436.
16. Quijada, M.A.; Rodríguez de Marcos, L.V.; Del Hoyo, J.G.; Gray, E.; Wollack, E.J.; Brown, A. Advanced Al mirrors protected with LiF overcoat to realize stable mirror coatings for astronomical telescopes. In Proceedings of the Advances in Optical and Mechanical Technologies for Telescopes and Instrumentation V, Montréal, QC, Canada, 17–23 July 2022; Geyl, R., Navarro, R., Eds.; SPIE: Bellingham, WA, USA, 2022; p. 66, ISBN 9781510653573.

17. Angel, D.W.; Hunter, W.R.; Tousey, R.; Hass, G. Extreme Ultraviolet Reflectance of LiF-Coated Aluminum Mirrors. *J. Opt. Soc. Am.* **1961**, *51*, 913. [[CrossRef](#)]
18. Willers, G.; Hagendorf, C.; Naumann, V.; Holzlöhner, R.; Guisard, S. Soiling induced nano-defects on aluminum telescope mirror coatings. *Appl. Opt.* **2022**, *61*, 2727–2732. [[CrossRef](#)]
19. Edmends, J.S.; Maldé, C.N.; Corrigan, S.J. Measurements of the far ultraviolet reflectivity of evaporated aluminum films under exposure to O<sub>2</sub>, H<sub>2</sub>O, CO and CO<sub>2</sub>. *Vacuum* **1990**, *40*, 471–475. [[CrossRef](#)]
20. Li, S.; Wang, F.; Wang, Z.; Zhou, H.; Huo, T. Effect of humidity on the performance of Al/LiF/eMgF<sub>2</sub> mirrors in the far ultraviolet spectrum. *Opt. Eng.* **2022**, *61*, 031205. [[CrossRef](#)]
21. Oliveira, C.M.; Retherford, K.; Conard, S.J.; Barkhouser, R.H.; Friedman, S.D. Aging studies of LiF-coated optics for use in the far ultraviolet. In *EUV, X-Ray, and Gamma-Ray Instrumentation for Astronomy X, Proceedings of the SPIE's International Symposium on Optical Science, Engineering, and Instrumentation, Denver, CO, USA, 18 July 1999*; Siegmund, O.H.W., Flanagan, K.A., Eds.; SPIE: Bellingham, WA, USA, 1999; pp. 52–60.
22. Rydalch, T.; Lewis, D.M.; Allred, D.D. Stability of lithium fluoride thin films as a function of humidity and temperature. In *Proceedings of the Advances in Optical and Mechanical Technologies for Telescopes and Instrumentation V, Montréal, QC, Canada, 17–23 July 2022*; Geyl, R., Navarro, R., Eds.; SPIE: Bellingham, WA, USA, 2022; p. 207, ISBN 9781510653573.
23. Ohl IV, R.G.; Barkhouser, R.H.; Conard, S.J.; Friedman, S.D.; Hampton, J.; Moos, H.W.; Nikulla, P.; Oliveira, C.M.; Saha, T.T. Performance of the Far Ultraviolet Spectroscopic Explorer mirror assemblies. In *Instrumentation for UV/EUV Astronomy and Solar Missions, Proceedings of the International Symposium on Optical Science and Technology, San Diego, CA, USA, 30 July 2000*; Fineschi, S., Korendyke, C.M., Siegmund, O.H.W., Woodgate, B.E., Eds.; SPIE: Bellingham, WA, USA, 2000; pp. 137–148.
24. Liu, C.; Guo, Q.; Cao, G.; Ai, W.; Guan, Y. Vacuum ultraviolet high-reflectance aluminum mirrors on copper substrate for application in noble liquid time projection chamber. *Vacuum* **2022**, *197*, 110806. [[CrossRef](#)]
25. Larruquert, J.I.; Honrado-Benítez, C.; Gutiérrez-Luna, N.; Ríos-Fernández, Á.; López-Reyes, P. Far UV-enhanced Al mirrors with a Ti seed film. *Opt. Express* **2021**, *29*, 7706–7712. [[CrossRef](#)]
26. UNIGIT. Grating Solver Software. Available online: <https://unigit.net> (accessed on 15 December 2022).
27. Quijada, M.A.; Rice, S.; Mentzell, E. Enhanced MgF<sub>2</sub> and LiF over-coated Al mirrors for FUV space astronomy. In *Modern Technologies in Space- and Ground-Based Telescopes and Instrumentation II, Proceedings of the SPIE Astronomical Telescopes + Instrumentation, Amsterdam, The Netherlands, 1 July 2012*; Navarro, R., Cunningham, C.R., Prieto, E., Eds.; SPIE: Bellingham, WA, USA, 2012; p. 84502H.
28. Quijada, M.A.; Del Hoyo, J.; Rice, S. Enhanced far-ultraviolet reflectance of MgF<sub>2</sub> and LiF over-coated Al mirrors. In *Space Telescopes and Instrumentation 2014: Ultraviolet to Gamma Ray, Proceedings of the SPIE Astronomical Telescopes + Instrumentation, Montréal, QC, Canada, 22 June 2014*; Takahashi, T., den Herder, J.-W.A., Bautz, M., Eds.; SPIE: Bellingham, WA, USA, 2014; p. 91444G.
29. Stempfhuber, S. Entwicklung von Breitbandig Hochreflektierenden Aluminiumschichten im VUV-Bereich. Ph.D. Thesis, Friedrich Schiller Universität Jena, Jena, Germany.
30. Shiles, E.; Sasaki, T.; Inokuti, M.; Smith, D.Y. Self-consistency and sum-rule tests in the Kramers-Kronig analysis of optical data: Applications to aluminum. *Phys. Rev. B* **1980**, *22*, 1612–1628. [[CrossRef](#)]
31. Wilbrandt, S.; Stenzel, O.; Liaf, A.; Munzert, P.; Schwinde, S.; Stempfhuber, S.; Felde, N.; Trost, M.; Seifert, T.; Schröder, S. Spectrophotometric Characterization of Thin Semi-Transparent Aluminum Films Prepared by Electron Beam Evaporation and Magnetron Sputtering. *Coatings* **2022**, *12*, 1278. [[CrossRef](#)]
32. Stenzel, O. *The Physics of Thin Film Optical Spectra: An Introduction*, 2nd ed.; Springer International Publishing: Cham, Switzerland, 2016; pp. 90–91, ISBN 978-3-319-21602-7.
33. Hagemann, H.-J.; Gudat, W.; Kunz, C. Optical constants from the far infrared to the x-ray region: Mg, Al, Cu, Ag, Au, Bi, C, and Al<sub>2</sub>O<sub>3</sub>. *J. Opt. Soc. Am.* **1975**, *65*, 742. [[CrossRef](#)]
34. He, J.Y. Modelling UV and VUV optical losses of rough aluminum films. Master's Thesis, Friedrich Schiller Universität Jena, Jena, Germany, 2022.
35. Jobst, P.J.; Stenzel, O.; Schürmann, M.; Modsching, N.; Yulin, S.; Wilbrandt, S.; Gäbler, D.; Kaiser, N.; Tünnermann, A. Optical properties of unprotected and protected sputtered silver films: Surface morphology vs. UV/VIS reflectance. *Adv. Opt. Technol.* **2014**, *3*, 91–102. [[CrossRef](#)]

**Disclaimer/Publisher's Note:** The statements, opinions and data contained in all publications are solely those of the individual author(s) and contributor(s) and not of MDPI and/or the editor(s). MDPI and/or the editor(s) disclaim responsibility for any injury to people or property resulting from any ideas, methods, instructions or products referred to in the content.